Peer-Reviewed Technical Communication

Distributed Traversability Analysis of Flow Field Under Communication Constraints

Shijie Liu, *Student Member, IEEE*, Jie Sun, Jiancheng Yu, Aiqun Zhang, and Fumin Zhang, *Senior Member, IEEE*

***Abstract*—Traversability analysis, previously developed for ground robots, is extended to be performed by a group of marine vehicles over ocean flow fields. To enable distributed path planning against flow, a systematic method is developed to determine a flow map that is significant for sharing among vehicles. Using traversability analysis, each vehicle finds a set of support vectors to approximate the boundary of flow regions with strong average flow speed. These support vectors, together with the parameters determined by the traversability analysis, are then shared over the communication links. The shared information is used by each vehicle to construct a flow map that supports path planning algorithms running on each vehicle. Underwater communication limits the amount of information contained in a map that can be shared among vehicles. A novel method for information reduction is developed so that only reduced flow maps are shared. The length of the data packets can be adjusted through an optimization process that balance between the fidelity of the approximated boundary and the number of bits that need to be transmitted. Simulation results demonstrate that the flow maps constructed from the shared information can have sufficient quality to allow near-optimal paths to be generated.**

***Index Terms*—Communication constraints, marine robotics, path planning, traversability analysis.**

I. Introduction

OCEAN sensing applications often favor the use of a fleet of marine vehicles that cooperate with each other [1], [2]. Planning paths for a swarm of marine vehicles are necessary tasks to coordinate their trajectories to increase the quality of data collected. A variety of path planning algorithms have been implemented for marine vehicles, including the A* algorithm [3], the genetic algorithm [4], the level set method [5], and the fast marching method [6]. The bottleneck for distributed path planning for marine vehicles is the constrained communication, which limits the amount of information that can be shared among vehicles. So far, existing works on cooperative or distributed path planning mainly focus on autonomous ground vehicles and unmanned aerial vehicles (UAVs). For instance, results in [7] require that each vehicle in the group has to share the kinematic and sensor information with others so that each vehicle can replan its path based on its own sensor data and those received from other vehicles. In [8], paths that avoid no-fly zones and obstacles for multiple UAVs are generated. These techniques are not directly applicable for marine vehicles due to the requirements on frequent information sharing among vehicles. A centralized approach for real-time trajectory generation of cooperating marine vehicles is presented in [9], where an exogenous system is employed to broadcast necessary information for path planning.

Our work is developed while considering realistic underwater communication constraints. Baccour *et al.* [10] give a comprehensive survey on link quality estimation of wireless sensor networks. Inspired by the efficiency measure in [11], we consider the stop and wait (S&W) scheme that is used for underwater communication, and our method shares flow information within single data packet. We introduce a quality metric that is used to determine the number of data bits that can be reliably transmitted over an underwater communication link. Since only a single packet is used for data transmission, a major challenge is to determine the most significant information that need to be shared to enable distributed path planning. It is not realistic for vehicles to share the complete map of flow; therefore, data compression/information extraction techniques are needed to generate a reduced map for sharing.

Traversability analysis, which has been previously applied to evaluate rough terrains for ground robots to determine whether an area can be safely accessed [12]–[18], is extended to evaluate flow fields for marine vehicles in this paper. For ground robots, traversability analysis is based on three parameters that characterize a rough ground surface: height, slope, and roughness. The height and the slope of the surface determine whether a ground robot can move through a region and how much time and energy it will consume in doing so. The roughness of the surface measures deviation from a smooth surface. Areas with large height, slope, and roughness are considered as obstacles to be avoided [18]–[21]. For a 2-D flow field, the average flow corresponds to the height and slope of a rough terrain, and the spatial variation of the flow provides a measure of the roughness of the flow field. Therefore, regions with strong average flow, as well as large spatial variations, are more significant for path planning. When a group of marine vehicles are considered, each vehicle should share these more significant regions with other vehicles, while less significant regions can be ignored. Guided by these insights, we propose a novel method for information reduction to allow the sharing of reduced flow maps among marine vehicles without violating the limits imposed by the communication links. Each vehicle uses the support vector data description (SVDD) [22] method

Manuscript received July 28, 2017; revised January 3, 2018; accepted March 22, 2018. This work was supported in part by the National Natural Science Foundation of China under Grants 61233013, 61673370, and 41376110; and in part by the State Key Laboratory of Robotics at the Shenyang Institute of Automation under Grant 2014-Z02. This paper was presented in part at the International Conference on Underwater Networks and Systems, Rome, Italy, 2014, and in part at the IEEE International Conference on Cyber Technology in Automation, Control, and Intelligent Systems, Shenyang, China, 2015. *(Corresponding author: Fumin Zhang.)*

Associate Editor: M. Chitre.

S. Liu and J. Sun are with the Shenyang Institute of Automation, Chinese Academy of Sciences, Shenyang 110016, China and also with the University of Chinese Academy of Sciences, Beijing 100049, China (e-mail: liushijie@sia.cn; sunjie@sia.cn).

J. Yu and A. Zhang are with the Shenyang Institute of Automation, Chinese Academy of Sciences, Shenyang 110016, China (e-mail: yjc@sia.cn; zaq@sia.cn).

F. Zhang is with the School of Electrical and Computer Engineering, Georgia Institute of Technology, Atlanta, GA 30332 USA (e-mail: fumin@gatech.edu).

Digital Object Identifier 10.1109/JOE.2018.2819758

to find a set of support vectors to represent the boundary of flow regions with strong average flow speed. These support vectors, together with the parameters for traversability, are then shared over the communication links. We show that the data length can be adjusted through an optimization process that seeks the balance between the fidelity of the approximated boundary and the number of bits that need to be transmitted.

Distributed traversability analysis is a novel contribution that enables distributed path planning for marine vehicles. In particular, the explicit tradeoff between the fidelity of the flow map and the communication constraint was not yet found in the literature. Some preliminary results are developed in our conference publications [23], [24], where the strong flow regions are treated as obstacles without leveraging traversability analysis. The extension made in this paper guarantee a feasible path to be generated by the path planning algorithm that also leverages strong flow regions that are traversable. In addition, this paper significantly improved the proposed communication quality measure in [24]. More thorough simulation results are also provided to demonstrate the effectiveness of our proposed method.

This paper is organized as follows. The problem of distributed path planning is formulated in Section II. In Section III, traversability analysis is performed and the SVDD method is used to find approximated representations of the boundaries of regions with strong flow. We also discuss how this information can be leveraged by the level set algorithm for path planning. A metric for communication link named the required link quality (RLQ) is introduced in Section IV. The RLQ provides a limit on the number of bits that can be transmitted. In Section V, we present simulation results of distributed path planning under the communication and traversability constraints.

II. Problem Formulation

For large-scale or high-resolution ocean observation, it is preferred to use a fleet of vehicles cooperating with each other for spatial and temporal coverage [25]. This often requires the paths of the vehicles to be coordinated to avoid under sampling or oversampling of certain area. Assume that a fleet of K vehicles $G_1, G_2, \ldots, G_K$ are deployed into the ocean at different locations. In this paper, we consider the planar trajectories, and the main external factor affecting the trajectories is the flow in the operation domain of the fleet. We assume that each vehicle has knowledge about the 2-D flow field within a small area around itself, which we call a patch. The flow information within a patch can be obtained by performing the objective analysis (OA), an optimal interpolation method that calculates the flow field based on the time series of flow measurements collected by the vehicle [26]. The reconstruction may cover a large area, but the local patch is determined to contain the flow region with the least amount of uncertainty (see Fig. 1). We can discretize the patch into $m \times n$ grid points indexed by (i, j). Consequently, the flow velocities in this patch can be represented by two $m \times n$ matrices $\mathbf{U} = \{u_{ij}\}_{m,n}$ and $\mathbf{V} = \{v_{ij}\}_{m,n}$, where u_{ij} denotes flow speed in the east/west direction at grid point (i, j) and v_{ij} denotes flow speed in the north/south direction at grid point (i, j). Let us denote the flow in this patch as $\mathbf{F} = [\mathbf{U}, \mathbf{V}]$.

We now consider that vehicle G_1 plans a minimum time path from its starting position $\mathbf{r}_b$ to a destination $\mathbf{r}_d$, as illustrated in Fig. 1. Due to limited speed, vehicles should avoid regions with strong flow. G_1 has its local flow map F_1, enclosed by the blue solid curve in Fig. 1. However, to avoid passing through nontraversable regions on the way to $\mathbf{r}_d$, G_1 needs to communicate with other vehicles hoping for information of strong flow. For marine vehicles, transmitting all the flow data within a patch over underwater communication link or satellite communication link, two major communication methods used in the ocean, is quite difficult. In addition, such communication is required to happen frequently since the path would need to be replanned every time G_1 acquires new information from another vehicle. Therefore, two problems need to be addressed: First, we need to determine how much information can be shared under realistic communication constraints; and second, what information are necessary for vehicle G_1 to plan a path that can avoid regions that are difficult to traverse. These two problems are coupled with each other.

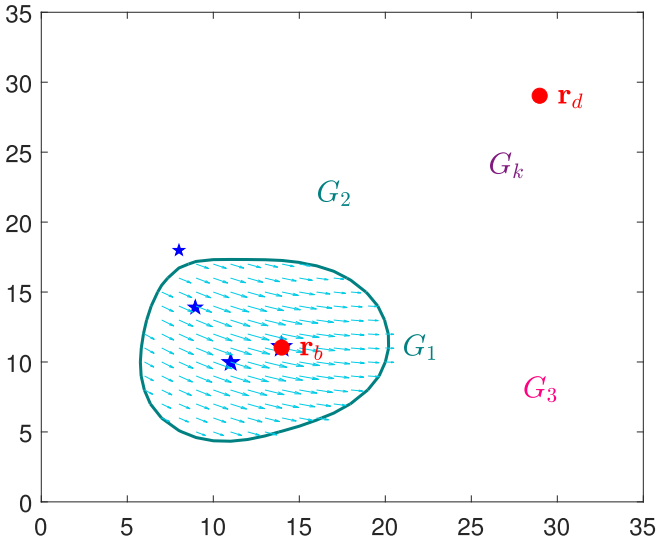

Fig. 1. For path planning from $\mathbf{r}_b$ to destination $\mathbf{r}_d$, vehicle G_1 only has knowledge about flow information in a local small patch. The patch is constructed by the OA using a time series measurements that contain the most recent measurements (the blue stars).

III. Traversability Analysis

This section introduces two methods used to extract the most significant information from the flow data of each vehicle that can be transmitted. First, a traversability analysis is performed to analyze the overall strength and "roughness" of the flow field within the patch of one vehicle. Then, the boundary of regions with flow strength exceeding a threshold, set to be less than the maximum speed of the vehicle, is represented using a small number of positions called the support vectors. The traversability parameters and the support vectors serve as the compressed information that cannot exceed a total number of bits, denoted as n_p^*, which will be determined from the quality of communication link introduced later in Section IV.

Taking vehicle G_2 for instance, suppose the local patch where flow information is available to G_2 contains a region Ω_2 where the average flow is strong. Then, Ω_2 is of great interest for sharing with others since flow in it would seriously affect a vehicle's motion. To meet the requirement of the communication link, the amount of flow data in Ω_2 will be reduced using the SVDD method where only the boundary of Ω_2 is extracted and shared with other vehicles. After receiving the reduced information, G_1 can approximately reconstruct the strong flow regions. The traversability parameters can then help to determine whether the region should be leveraged, or should be completely avoided by a path planning algorithm.

A. Traversability of a Flow Field

Three traversability parameters are often used by mobile robots to analyze a terrain: the height, slope, and roughness. Analogously, we

introduce two parameters for the traversability analysis over a flow field. First, we define the average flow over a region Ω_2 to be

$$\bar{\mathbf{f}}_{\Omega_2} = (\bar{u}_{\Omega_2}, \bar{v}_{\Omega_2}) = \left(\frac{1}{N_{\Omega_2}} \sum_{i,j \in \Omega_2} u_{ij}, \frac{1}{N_{\Omega_2}} \sum_{i,j \in \Omega_2} v_{ij} \right)$$

where u_{ij} (v_{ij}) is the value of $u(v)$ at grid point (i, j) and N_{Ω_2} is the total number of grid points in Ω_2. The average flow resembles the height and the slope of a terrain on the ground. Next, we introduce the roughness of a flow field as the maximum of the two standard deviations of the flow in the two dimensions

$$r_f = \max \left(\sqrt{\frac{1}{N_\Omega} \sum\nolimits_{i,j \in \Omega} (u_{ij} - \bar{u}_\Omega)^2}, \sqrt{\frac{1}{N_\Omega} \sum\nolimits_{i,j \in \Omega} (v_{ij} - \bar{v}_\Omega)^2} \right).$$

The average flow indicates the strength and direction of flow in the region. Most path planning algorithms actually produce paths that move along with strong flows, instead of going against them. The roughness of the flow reflects the uncertainty in the flow field. High roughness indicates that the flow in the region may change in direction or magnitude over a small spatial scale, which may alter the trajectories of vehicles unpredictably. Most path planning algorithms will have difficulty producing feasible paths in rough flow fields with strong average flow.

The thresholding method for traversability evaluation in the mobile robotics literature [17]–[19] can now be applied to the flow field. A threshold for the roughness can be set to decide whether it is safe to pass through a flow field or not. If the roughness r_f exceeds the threshold, then the vehicle should avoid the flow region due to the strong spatial variations. On the other hand, a threshold for the average flow strength can be set as a portion of the vehicle speed to determine whether the flow is strong enough to have high impact on path planning. Regions with average flow speed that exceeds the threshold should be shared with other vehicles so that the path planning algorithms will be able to benefit from the knowledge.

B. Boundary of Region With Strong Flow

Once the threshold for the average flow strength is determined, we can use the SVDD method to determine the boundary of the flow region where the average flow speed exceeds this threshold. As reviewed in Section III–VI, a set of support vectors are produced by SVDD to represent the boundary that separates the positions with strong flow [the target points] from the positions with weak flow [the outliers]. Each support vector is a position $\mathbf{x}_i$ on the boundary together with a positive weight $\alpha_i^* > 0$. The collection of all support vectors is a set S. SVDD performs data reduction because it produces only a small number of support vectors from which the boundary between the target points and the outliers can be reconstructed. The number of support vectors representing the boundary can be adjusted by tuning the width parameter σ of the Gaussian kernel function K_G used for the SVDD [see the Appendix]. This in turn determines the length of data that needs to be transmitted to other vehicles. More support vectors give better accuracy representing the boundary, but require larger packet size and higher data rate in communication. In this section, we determine an optimal σ to balance the packet size for communication and the representation error of the SVDD method.

We introduce the representation error E of SVDD that contains two components: e_1, the target rejection error, indicates how many target points are wrongly rejected; and e_2, the outlier acception error, indicates how many outlier points are wrongly accepted. To calculate these two errors, a set of N test points are selected in the patch of a vehicle and then tested against the reconstructed boundary. If the point is a target point but is located outside of the boundary, then the target point is wrongly rejected. If the point is an outlier but is located inside the boundary, then the point is wrongly accepted. Let N_r be the number of target points that are wrongly rejected and N_a be the number of outlier points that are wrongly accepted. Then $e_1 = N_r/N$ and $e_2 = N_a/N$. Specifically, we formulate a constrained optimization problem as follows:

$$\min_{\sigma} \; E = e_1 + e_2 \tag{1}$$

under the constraint

$$c(4 + 2N_S) \leq n_p^* \tag{2}$$

where n_p^* is the maximum number of data bits determined by the communication link. On the left-hand side of this inequality, N_S represents the number of the support vectors and their corresponding weights for a specific σ, the value 4 represents the traversability parameters that need to be coded, which include the width of Gaussian kernel σ, the average flow $\bar{u}_{\Omega_2}$ and $\bar{v}_{\Omega_2}$, and the roughness of flow r_f. The term c is the number of bits needed for coding each parameter.

The optimization problem (1) can be first solved without considering the constraint (2). Suppose the resulting σ^* achieves the minimal error E, i.e., $\sigma^* = \text{argmin}_\sigma \{E\}$. Select the optimal σ^* and then determine the number of support vectors resulted by N_S^*. Now considering the constraint (2), if N_S^* satisfies the constraint, then σ^* is the desired solution. Otherwise, if N_S^* does not satisfy the constraint, then the value of σ will be increased from σ^* to compute a new N_S until the constraint is satisfied.

C. Flow Map for Path Planning

As a result of traversability analysis, a flow map will be constructed by each vehicle for path planning. The flow map will contain the local patch and the reconstructed map outside of the local patch. Taking vehicle G_1 as an example, after receiving the compressed flow information from other vehicles, vehicle G_1 should first reconstruct the strong flow region using the set of support vectors S and their corresponding α_s^*. G_1 computes the boundary of the strong flow region using (17), and checks whether a position is enclosed by the boundary or not using (18). All positions that are enclosed by the boundary have strong flow. For each strong flow region, the roughness of the flow in this region is then considered. If the roughness r_f is within a preset threshold, then the region will be filled with the average flow; otherwise, the region will be considered as an obstacle for path planning to avoid.

For a path planning algorithm such as the level set method used in the following sections, the planned path will contain two segments. One segment is in G_1's local patch, the other is outside of this patch where the flow is only partially known. If a region is viewed as an obstacle, the algorithm will prevent a path from entering this region.

A flow map constructed distributedly may contain "holes," e.g., regions where no flow information is available at all. These holes can be temporarily filled with average flow or even no flow. Note that the existence of "holes" is not a problem caused by the traversability analysis. It is rather a practical challenge for any method of flow map construction. While vehicles are moving, the amount of information collected will be increasing, and we expect the "holes" can be filled eventually as more data being collected.

IV. Single Packet Transmission

The difficulty in communication in a marine environment would limit the transmission of information. The S&W scheme is a popular method for underwater communication. This protocol requires that the transmitter, say vehicle G_2, stops and waits for an acknowledgment response from vehicle G_1 after sending a message to it. Through this handshaking process, the link quality between vehicles G_2 and G_1 can be measured. Since the S&W protocol is of low efficiency, a strategy to avoid overhead is for G_2 to pack all the necessary data for path planning into a single packet of several hundred bits, and then transmit this packet to G_1 after the testing phase of the communication link is done [11]. This single packet strategy is feasible for sharing flow information that is generated by traversability analysis. Since the flow map for path planning needs to be reconstructed relatively frequently, using a single packet strategy can maintain the integrity of the flow map when packet loss happens. On the other hand, the single packet strategy put a limit on the number of bits within one packet that can be used for information sharing. Our goal is to determine the largest number of bits n_p^* that is used as a constraint for traversability analysis.

A. Measuring Link Quality

Since communication link changes over time, its quality needs to be measured by the S&W every time a link is established. In general, the following three main components can be measured.

1) Bit error ratio (BER) p: BER is the number of bit errors divided by the total number of bits in a received packet.
2) Packet delay t_d: Packet delay t_d is the time needed to transmit a packet from source to destination. Packet delay not only reflects the transmission time in between the sender and the receiver, but also reflects the probability for a packet to be lost (e.g., the packet loss ratio) during the transmission. This is because under the S&W protocol, any packet that gets lost will be retransmitted until successfully received.
3) Packet delay variation $\mathrm{Var}(t_d)$: Due to uncertainties in the channel, the packet delay t_d is also random. The variation of t_d represents the deviation between actual packet delay and average packet delay.

After a link has been established between two vehicles, say G_2 and G_1, G_2 sends G_1 a testing packet which contains n bits. $n = n_h + n_d + n_t$, where n_h bits are allocated for the header bits, n_d bits are allocated for data bits, and n_t bits are allocated for the tail bits. The n_d data bits for the testing packet contain a predefined sequence which is known to both the transmitter and the receiver. When G_1 receives the packet, it checks the bit error and records the BER as p_s, also called sending BER. Immediately, G_1 starts a new test packet with its n_t tail bits filled with p_s as a responding packet to send back to G_2. After receiving this response, G_2 checks the BER p_r, also called returning BER, and use p_s together with p_r to estimate the BER for the link as

$$p = 1 - (1 - p_s)(1 - p_r).$$

For a packet that contains n_d data bits, the probability for the entire packet to have error is then estimated as

$$P = 1 - (1 - p)^{n_d}. \tag{3}$$

For G_2 to measure the packet delay t_d and the packet delay variation $\mathrm{Var}(t_d)$, it can measure delay times $\{t_{d_i}\}$ for sending $i = 1, 2, \ldots, m$ packets. Then, t_d can be estimated by letting $t_d = (1/m)\sum_{i=1}^{m} t_{d_i}$, and the variance of packet delay can be calculated by

$$\mathrm{Var}(t_d) = \frac{1}{m}\sum_{i=1}^{m}(t_{d_i} - t_d)^2. \tag{4}$$

B. Required Link Quality

Let n_p be the number of data bits within the single packet that carry the information of the flow that is to be shared. Due to the BER p, we must require

$$n_p \le n_d(1-p)^{n_d}$$

for reliable transmission and receiving. Inspired by Stojanovic [11], we consider the "efficiency index" as

$$\lambda(n_p) = \frac{n_p T_s}{t_d} \tag{5}$$

where T_s is the time required to transmit and receive 1 b it, and t_d is the average time delay for transmitting one packet. This efficiency index measures the ratio between the time spent to transmit the effective bits and the total time spent for single packet transmission. Note that in [11], the efficiency index is defined as the upper bound of λ [e.g., $(n_d T_s/t_n)(1-p)^{n_d}$] so that the optimal length of data bits n_d can be determined to achieve maximum efficiency. In this paper, we assume that the packet size n_d is already known for all the vehicles. Hence, we modified the definition of efficiency to focus on finding the n_p number of bits within a packet that can be allocated for information that will be used for path planning.

We define a quality metric named the RLQ that measures the capability of sending n_p bits reliably in one packet that contains n_d data bits

$$\mathrm{RLQ}(n_p) = \lambda(n_p)(\kappa_1 \mathrm{Var}(t_d) + \kappa_2 P) \tag{6}$$

where $\mathrm{Var}(t_d)$ represents the variation in the packet delay defined in (4), P represents the probability for a packet to have error defined in (3), and λ is the efficiency index defined in (5). The weights κ_1 and κ_2 are positive regulating factors that will be chosen so that the $\mathrm{RLQ}(n_p)$ is easy to be interpreted. In our simulation work, we have chosen κ_1 and κ_2 so that the RLQ is between 0 and 10 for all possible $\mathrm{Var}(t_d)$ and P. If a link has constant $\mathrm{Var}(t_d)$ and P, then larger n_p leads to higher efficiency λ, but requires higher RLQ. If either the $\mathrm{Var}(t_d)$ or P becomes larger, then the RLQ for sending a packet with the same size becomes higher.

The main reason to introduce the RLQ as a function of n_p is to allow a convenient way for the data compression algorithms to determine what is the maximum number of data bits that can be shared among vehicles, based on the quality measured from the S&W protocol. Suppose the link quality is bounded above by a threshold $\bar{Q}$, then the maximum number of data bits that can be transmitted reliably can be determined as follows. First, find the largest allowed n_p such that

$$\mathrm{RLQ}(n_p) \le \bar{Q}.$$

At the same time, we need to guarantee enough redundancy by requesting that

$$n_p \le n_d(1-p)^{n_d}$$

to be satisfied. RLQ is monotonically increasing as n_p increases. The BER p is usually time varying due to uncertainty in the channel. We can find the maximum n_p^* from the two inequalities and then use it to formulate the constraint for data compression in (2).

We would like to point out that the RLQ can be estimated through measurements made by the vehicles during the process of establishing

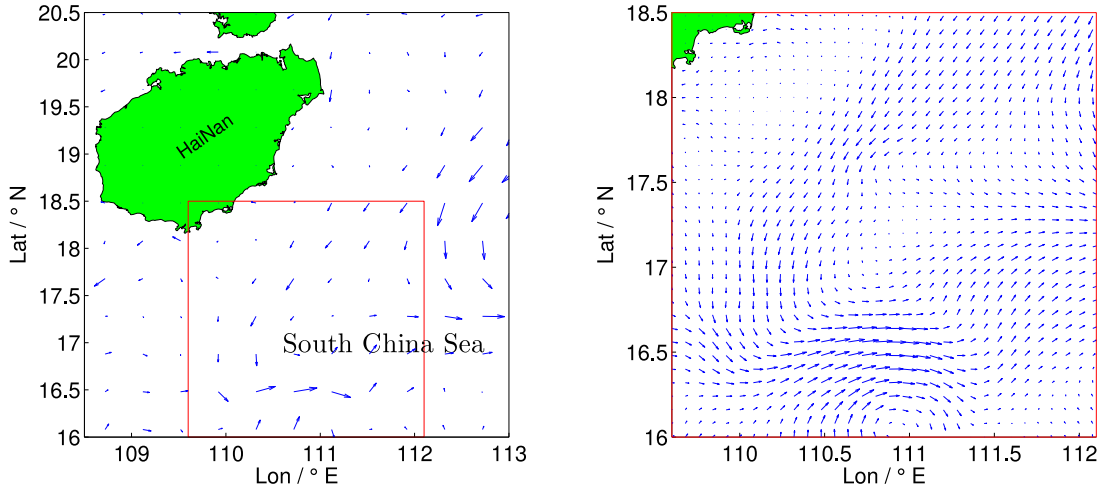

Fig. 2. Region in the South China Sea near the Hainan Island is shown. (a) Flow field obtained from HYCOM+NCODA Global $1/12^\circ$ analysis provided by the U.S. Naval Research Lab. (b) Interpolated flow field based on the HYCOM data with higher spatial resolution, where flow arrows are plotted shorter for better visibility. The date for the snapshots is February 22, 2017.

the communication link. The RLQ will be a time-varying function that will lead to a time varying n_p^*. The length of data for path planning should be smaller than n_p^*. On the other hand, the threshold $\bar{Q}$ is a design factor that needs to be determined beforehand. It can be first set at a relatively low value. If the communication is working well, then $\bar{Q}$ can be gradually increased to allow more data bits to be allocated for sharing flow maps.

V. Simulation Study

We simulate a fleet of four vehicles G_1, G_2, G_3, and G_4 that are deployed into a region in the South China Sea near the Hainan Island, as illustrated in Fig. 2. The flow field shown in this region is obtained from HYCOM+NCODA Global $1/12^\circ$ analysis provided by the U.S. Naval Research Lab, Washington, DC, USA [27]. This region is chosen due to the interesting spatial structure that belongs to part of a cyclone. The flow field in this region demonstrates strong spatial variation in both strength and directions. We assume that the maximum speed of the vehicles is 0.3 m/s. Then, the large flow in the southern part of the region is up to 0.6 m/s, exceeding the speed of the vehicles by 0.3 m/s.

A. Simulation Setup

For the purpose of supporting path planning simulations, we need to add data with higher spatial variation to the flow field data set to generate the "true" flow field. The resulting flow field may not accurately reflect the real ocean flow in the South China Sea region, but it nevertheless can support simulation studies to evaluate and verify the proposed distributed traversability analysis algorithms. The spatial resolutions of the combined flow field are increased by using the data-driven method used in [28] where Gaussian radial basis functions are employed for interpolation. The interpolated flow field is used as the "true" flow for the vehicles to measure in the simulation study. Note that our proposed method works well with the time-varying flow field. However, we do not introduce temporal variation in the "true" flow only because the temporal variation will add to the difficulty in explaining the simulation results.

We further simulate the tradeoff between accuracy and communication constraints for underwater data transmission. A statistical channel model [29] is utilized to simulate the effect of channel

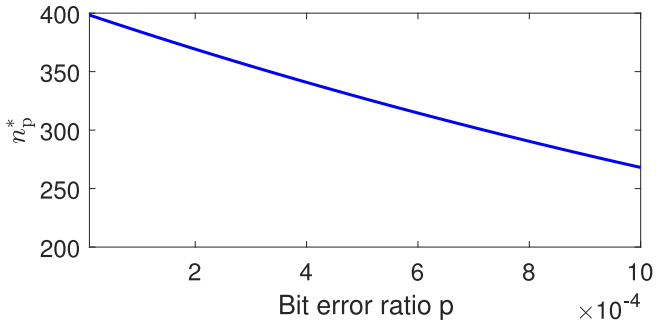

Fig. 3. Effective data bits n_p^* when BER p varying from 10^{-5} to 10^{-3}.

variation using the binary phase-shift keying modulation scheme [30]. The packet size is fixed at $n_d = 500$ b. Assume that, for simplicity, the communication links between G_1 and the other three vehicles have identical quality. Thus, under a specific BER p, the allowed upper bound of n_p for G_2, G_3, and G_4 is equal. We first set the range of the parameters for the communication link as $p \in [10^{-5}, 10^{-3}]$, then $P \in [0.004, 0.3298]$, according to (3). We set $\mathrm{Var}(t_d) \in [10^{-4}, 10^{-2}]$ and $t_d = 52$ s. We assume that the time taken to process 1 b information is $T_s = 10^{-7}$. Then, the κ_1 and κ_2 should be chosen so that $\mathrm{RLQ}\{n_d | t_d = 52\,\mathrm{s}, \mathrm{Var}(t_d) = 0.01, P = 0.3298\} = 10$. Meanwhile, we set $\kappa_1 \cdot (10^{-2} - 10^{-4}) = \kappa_2 \cdot (0.3298 - 0.004)$ to balance the influences on the RLQ from $\mathrm{Var}(t_d)$ and P. Then, an approximate solution for the parameters can be found as $\kappa_1 = 3.9 \times 10^9$ and $\kappa_2 = 1.3 \times 10^6$. Based on this knowledge, we select the threshold $\bar{Q}$ to be 8 to emulate a nonideal communication link that will be used by the vehicles. To determine the maximum number of data bits that are permitted by $\bar{Q}$, we solve the n_p from $\mathrm{RLQ}(n_p) = \bar{Q}$.

We simulate the communication links with the value of p changing from 10^{-5} to 10^{-3}. With each value of p, the time delay $t_d = 52$ s and $\mathrm{Var}(t_d) = 0.006$. Fig. 3 depicts the effective data bits n_p^* decreasing as the BER p increases from 10^{-5} to 10^{-3}. The allowed upper bound of N_S, the number of support vectors, in the constraint equation (2) under each p can be computed by $N_S = \lfloor (n_p^*/c - 4)/2 \rfloor$. The value c is the number of bits to encode a data point and set to be 20 b in the simulation. Each support vector will take 40 b to encode, and each

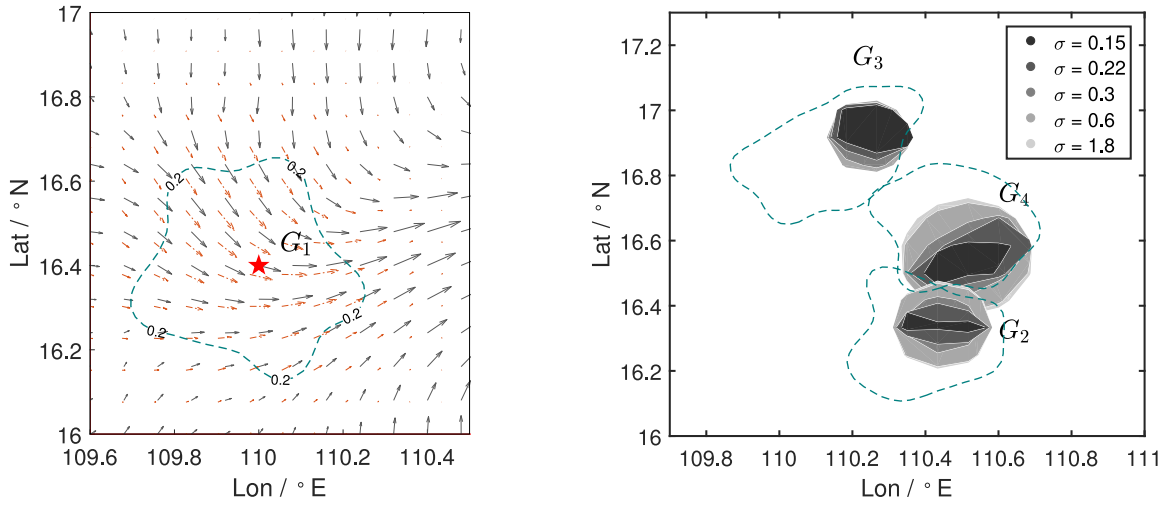

(a) (b)

Fig. 4. (a) G_1 uses its latest measurements to estimate the flow field around its current position. The solid gray arrow depicts the true flow and the dashed red arrow depicts the estimated flow. The region with uncertainty lower than 0.2 is then viewed as the local patch of this vehicle, which is marked by dashed boundary. (b) Boundaries of the high-flow regions for G_2, G_2, and G_4 are shown for different values of the width of the Gaussian kernel σ.

weight will also take 20 b to encode. In the following simulations, the BER will be set to $p = 4 \times 10^{-4}$, which corresponds to the maximum number of supporting vectors being $N_S = 7$.

B. Step 1: Data Compression

Each simulated vehicle is able to collect a sequence of measurements of the flow along its trajectory. Each vehicle then estimates the flow field using the OA method that provides an optimal prediction of spatial distributions given measurements at finite spatial locations [31]. In addition, OA also computes uncertainty associated with the spatial prediction. This value of uncertainty is between $[0, 1]$ while 1 indicates the highest uncertainty. The reconstructed flow in the local patch of vehicle G_1 is marked by red arrows in Fig. 4(a), while the "true" flow is marked by blue arrows for comparison. The dashed green line represents the boundary of the local patch where the uncertainty is less than 0.2. We can observe a good match between the true flow and the reconstructed flow. The value 0.2 can be chosen as other small values, which will not affect the conclusions. Within each local patch, the high-flow regions where flow speed is greater than a threshold 0.3 m/s, which is the depth averaged speed for the vehicles, will be compressed by SVDD to share with other vehicles. At the starting time, vehicle G_3 does not have a high-flow region. The boundaries of the high-flow regions produced by SVDD with different σ values are illustrated for G_2 and G_4 in Fig. 4(b). We can clearly observe that as the values of σ increase in both cases, the shape of the high-flow regions becomes more circular, losing the accuracy in representing the boundary.

Now we demonstrate how vehicles G_2 and G_4 will determine the compression of the high-flow region in their local patches. The optimal width of the Gaussian kernel σ for SVDD with p increasing from 10^{-5} to 10^{-3} is shown in Fig. 5. For G_2, the minimum representing error occurs when $\sigma^* = 0.24°$, and the resulting $N_S^* = 5$ when $p \in [10^{-5}, 5.6 \times 10^{-4}]$. Then, the optimal number of support vector N_S^* is less than the upper bound 7. For G_4, the optimal $\sigma^* = 0.35°$ but its corresponding $N_S^* = 9$. Since $N_S^* > 7$, we have to increase the value of σ to 0.41° so that $N_S^* = 7$. For G_3, the optimal $\sigma^* = 0.27°$ and its corresponding $N_S^* = 7$.

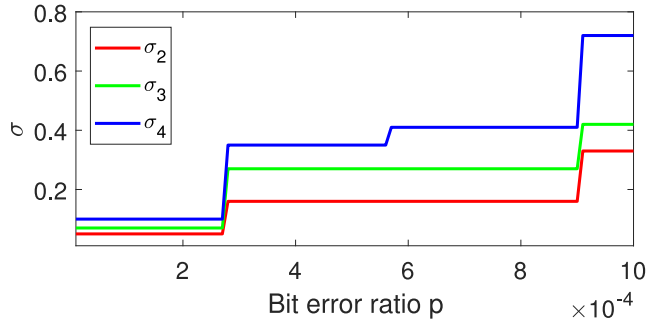

Fig. 5. Value of σ for transmitters with changing BER p from 10^{-5} to 10^{-3}.

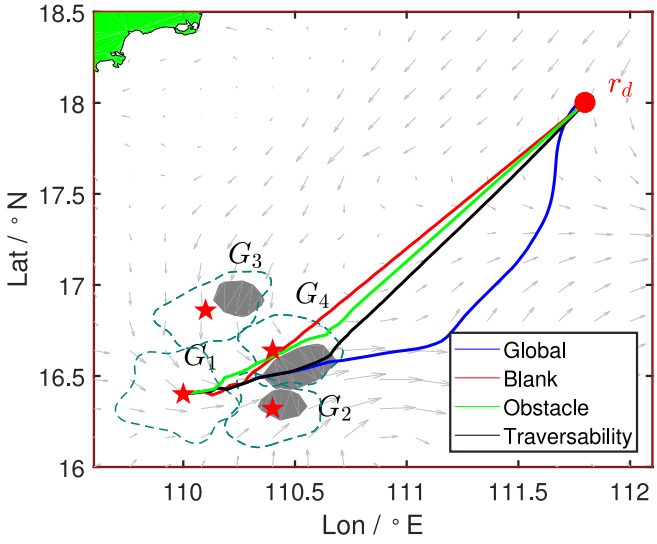

Fig. 6. Path planning in four cases. In the "Global" case, as a comparison, G_1 plans a path (in blue) using the knowledge of the entire flow field. In the "Blank" case, G_1 assumes no flow outside of its local patch in path planning. In the "Obstacle" case, G_1 uses shared information from others. The recognized high-flow regions, without traversability analysis, are all considered as obstacles. In the "Traversability" case, G_1 reconstructs flow field using the information from other vehicles that have performed traversability analysis.

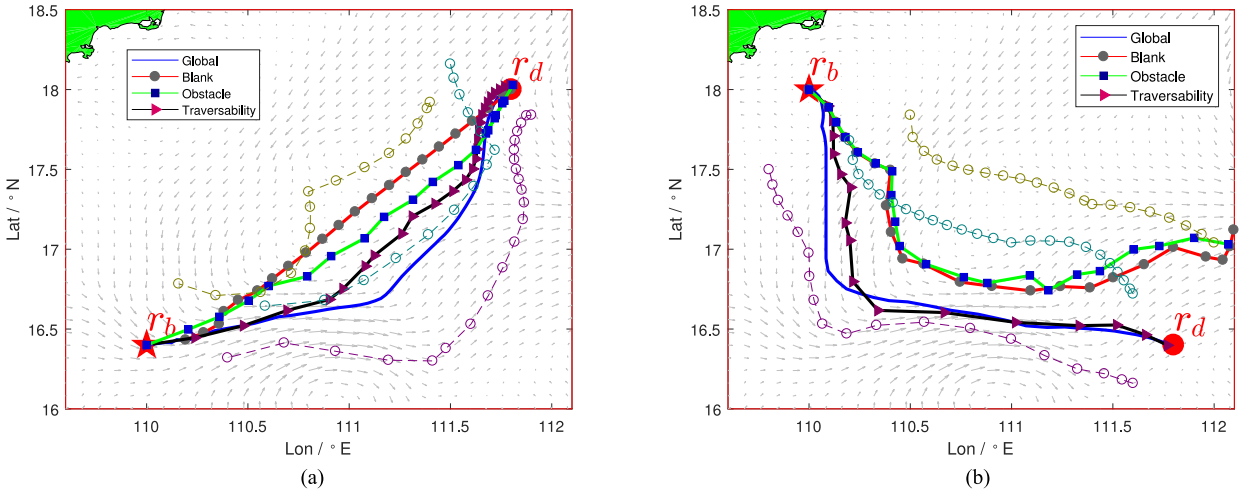

Fig. 7. Paths followed by the four vehicles in two simulations. (a) G_1 travels from the lower left corner to the upper right corner. (b) G_1 travels from the upper left corner to the lower right corner. The solid line paths illustrate the paths followed by G_1 in four different cases. The fixed trajectories of the other three vehicles are illustrated by dashed lines with markers.

Other than the choice of σ and the number of supporting vectors, each vehicle will compute the parameters for traversability, e.g., the average u, v, and the roughness r_f as follows: G_2: (0.39, 0.12, 0.00085); G_3: (0.03, 0.34, 0.00017); and G_4: (0.42, 0.08, 0.00049). These values, together with the σ values and the support vectors, are transmitted to all other vehicles.

C. Step 2: Path Planning

After receiving the shared flow maps together with the parameters for traversability from other vehicles, G_1 reconstructs its flow field for path planning. The threshold of roughness of flow field is set to be 0.001, which is a value that can be chosen by design. At this point of time, the flow from G_2 and G_4 with low roughness is represented by the average flow.

We use the level set method to plan time optimal paths from the initial location of G_1 to destinations diagonally across the region, as shown in Fig. 6. This figure demonstrates the moment at the beginning of the simulation where all four vehicles are at their initial positions. The paths are planned for four cases, each corresponding to a different way of using the flow map. These paths planned by G_1 are compared. In the first case, the path is planned using the complete flow information from the entire domain. We label this case as "Global" and use it as a benchmark for the other three cases. The "Global" path is plotted as a blue line in Fig. 6. The second case is when G_1 only uses flow information from its local patch, this corresponding to the case where no communication happens among the vehicles. We label this case as "Blank." The planned path is plotted as red lines in Fig. 6. The third case uses the method in our previous work [23] where the recognized strong flow regions are all regarded as obstacles that need to be avoided. This case is labeled as "Obstacle" and the path is plotted as a green line in Fig. 6. The fourth case uses the method developed in this paper where traversability analysis is used to determine whether a strong flow region can be leveraged or not. This case is labeled as "Traversability," and the path is plotted as a black line in Fig. 6. We can observe that the Global path is not the shortest path, and the Traversability path is the one that is the most similar to the Global path.

D. Evaluating Path Planning Performance

The two steps, data compression and path planning, are performed iteratively by all vehicles while they are following the planned paths to their destinations. We will now evaluate the performance of the vehicles when the distributed traversability analysis is employed. To simplify the evaluation process, we assume that vehicles G_2, G_3, and G_4 will follow fixed paths. We allow vehicle G_1 to replan its path after it has reached the boundary of its local patch. Its own local patch will be reconstructed with more recent measurements, and its flow map will be updated by using information received from other vehicles. Since all vehicles are moving and sharing information, G_1 will have better information about the flow field as it moves from the starting position to the ending position. Again, G_1 will plan its paths for four cases: the Global, the Blank, the Obstacle, and the Traversability cases. We will compare the entire path that G_1 will trace out from the starting position to the ending position.

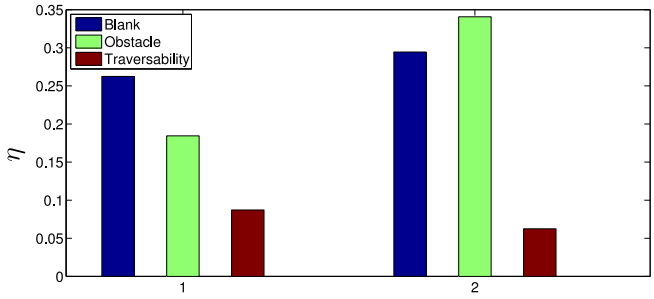

Fig. 8. η values of the paths followed by G_1 for the two scenarios in Fig. 7. The left three bars correspond to Fig. 7(a) and the right three bars correspond to Fig. 7(b). The traversability paths have the smallest values in both cases.

We evaluate the performance of the paths in the Blank, the Obstacle, and the Traversability cases by comparing them with the "Global" case where the path is optimal since all flow information is used for path planning. Our intuition is that a path is better if it is closer to that of the "Global" case. We define a metric η to quantitatively evaluate the performance of a path γ as

$$\eta = \frac{\int |\gamma - \gamma_0| d\gamma}{|\gamma_0|^2}.$$

The less the value of η, the better the path is.

We plot the paths where the starting and ending positions for G_1 are selected, as shown in Fig. 7(a) and (b). Other than the four paths

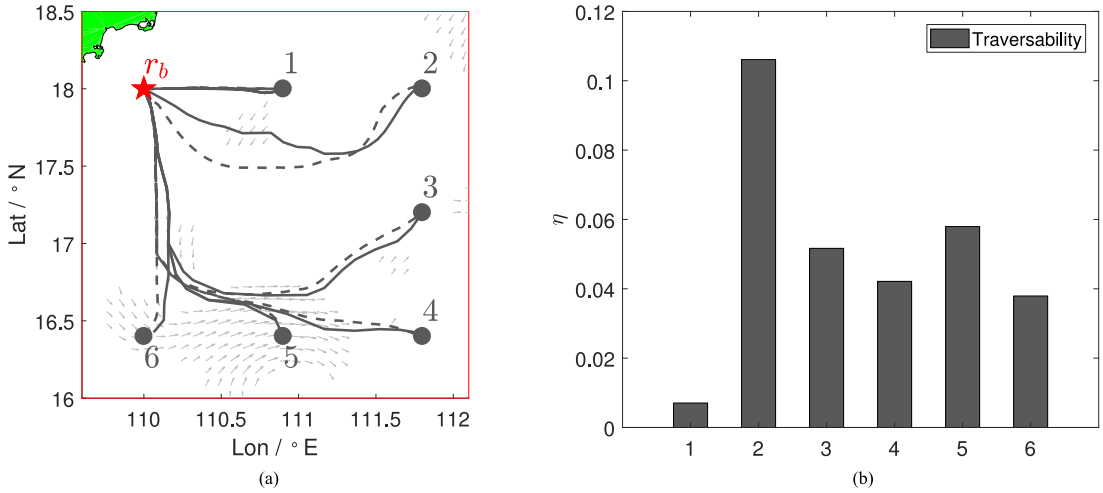

Fig. 9. Path followed by the vehicle to a set of destinations. (a) Global path and the Traversability path are compared for each destination. (b) η values for the Traversability paths are plotted and compared.

traced by G_1 in each of the figures, we plot the fixed paths traced by the other three vehicles as well; these paths are the same in all four cases. Meanwhile, the η values of the paths for the three cases in Fig. 7(a) and (b) are compared in Fig. 8. It can be observed that the Traversability paths have the smallest η values in all comparisons.

In Fig. 7(a) and (b), the Traversability path successfully leverages the high-speed and beneficial flow. In Fig. 7(b), since crucial flow information is missing from all three cases except in the "Global" case, the paths planned in the "Obstacle" case and "Blank" case finally fail to reach the destination. This indicates that by incorporating the traversability analysis, the performance of the path planning algorithm is improved.

E. Effect of Missing Information

To study how the missing flow information by data compression will affect the performance of the planned path, we select a number of destinations where paths are planned assisted by the traversability analysis, and compare them with the optimal paths. From the starting position in Fig. 7(a), we plan paths to a collection of destinations as illustrated in Fig. 9(a). For each destination, we compare the "Global" path and the "Traversability" path. Here, the Traversability path is computed by assuming that the vehicle knows the traversability parameters of all high-flow regions in the area; this assumption allows us to focus on one vehicle and ignore other vehicles.

The η values for each of the Traversability paths are plotted in Fig. 9(b). We can observe that the value is the highest for destination 2 in Fig. 9(a). This high value indicates that the missing information of the lower flow regions have greater effects on the path planned for destination 2 than the other destinations. For destination 2 in Fig. 9(a), the Traversability path goes through a high-flow region because it is not aware of a favorable low-flow region below the Traversability path that can be leveraged to speed up the travel. This illustrates that the missing favorable low-flow regions ignored by the traversability analysis can alter the paths to a certain extent.

VI. Conclusions and Future Works

This paper has demonstrated that data compression of the flow information shared by marine vehicles is feasible for distributed path planning under communication constraints. A key contribution is the method of determining the number of bits that can be transmitted based on measurements of the link quality. Even though this method is only developed for the S&W protocol, there may be ways to extend the ideas to other networking protocols. This paper also extended traversability analysis for marine vehicles over 2-D flow field. To the best of our knowledge, it is the first time that such traversability analysis is used to support path planning for ocean flow fields. It is reasonable to expect more results to be developed along this direction. This problem may be generalized to the 3-D settings and for more complex flow fields. Furthermore, our method based on SVDD adjusts the quality of the reduced flow map according to communication constraints. This code-sign approach tries to strike a balance between information needed for accurate path planning with the limitation of the communication constraints. We will perform experimental efforts to further investigate this tradeoff.

Appendix
Review of Support Vector Data Description

Suppose that one would like to extract some special data points from a data cluster from other data points. We refer the points that need to be extracted as "targets" and the other points as "outliers." In this paper, the target points are positions with strong flow, e.g., where the flow speed exceeds a certain threshold, and the outliers are positions with weaker flow.

The SVDD method produces a representation of the data cluster by searching for the smallest hypersphere that contains as many targets as possible but does not include outliers. Assume that a set of training data are given that contain targets $\{\mathbf{x}_i, i = 1, 2, \ldots, N\}$. The optimal hypersphere around $\{\mathbf{x}_i\}$ with center $\mathbf{a}$ and radius R can be obtained by minimizing the following function [22]:

$$\min_{R,\mathbf{a},\xi_i} \; F(R, \mathbf{a}, \xi_i) = R^2 + C \sum_{i=1}^{N_t} \xi_i \tag{7}$$

with the constraint

$$\|\mathbf{x}_i - \mathbf{a}\|^2 \leq R^2 + \xi_i \tag{8}$$

where $\xi_i \geq 0$ are slack decision variables that allow some targets to be excluded from the hypersphere. The parameter C is a weight that controls the tradeoff between the volume of the sphere and the number of targets excluded by the sphere.

To solve this constrained optimization problem, the Lagrange multiplier method is used to construct a function called the Lagrangian as follows:

$$L(R,\mathbf{a},\alpha_i,\xi_i,\gamma_i) = R^2 + C\sum_i \xi_i - \sum_i \alpha_i \left\{R^2 + \xi_i - \left(\|\mathbf{x}_i\|^2 - 2\mathbf{a}\cdot\mathbf{x}_i + \|\mathbf{a}\|^2\right)\right\} - \sum_i \gamma_i\xi_i \quad (9)$$

where $\alpha_i \geq 0$ and $\gamma_i \geq 0$ are the Lagrange multipliers. Setting partial derivatives of R, a, and ξ_i to zero gives the constraints

$$\frac{\partial L}{\partial R} = 0 : \sum_i \alpha_i = 1 \quad (10)$$

$$\frac{\partial L}{\partial \mathbf{a}} = 0 : \mathbf{a} = \sum_i \alpha_i \mathbf{x}_i \quad (11)$$

$$\frac{\partial L}{\partial \xi_i} = 0 : C - \alpha_i - \gamma_i = 0. \quad (12)$$

Substituting conditions (10)–(12) into the Lagrangian (9) results in

$$\hat{L} = \sum_i \alpha_i(\mathbf{x}_i \cdot \mathbf{x}_i) - \sum_{i,j} \alpha_i\alpha_j(\mathbf{x}_i \cdot \mathbf{x}_j). \quad (13)$$

The optimization problem then can be converted into its dual problem

$$\max_{\alpha_i} \hat{L}(\alpha_i)$$

which requires $\hat{L}$ to be maximized with respect to α_i.

Maximizing (13) with respect to α_i gives solutions α_i^* for $i = 1, 2, \ldots, N$. In practice, a large number of α_i^* become 0. The target points $\mathbf{x}_i$ with their corresponding $\alpha_i^* > 0$ are called support vectors. Define a set $S = \{\mathbf{x}_i | \alpha_i^* \neq 0\}$, which contains a smaller number of data points to represent the boundary of the data cluster. The center of the boundary sphere can be represented as a linear combination of all the support vectors as

$$\mathbf{a}^* = \sum_s \alpha_s^* \mathbf{x}_s \text{ where } \mathbf{x}_s \in S$$

and the radius of the boundary sphere can also be represented by any one of the support vectors as

$$R^{*2} = \|\mathbf{x}_s - \mathbf{a}^*\|^2.$$

A test point $\mathbf{z}$, which can either be a target or an outlier, is considered inside the boundary sphere when its distance to the center $\mathbf{a}$ of the boundary sphere is smaller than or equal to the radius R^* as

$$\|\mathbf{z} - \mathbf{a}^*\|^2 = (\mathbf{z}\cdot\mathbf{z}) - 2\sum_s \alpha_s^*(\mathbf{z}\cdot\mathbf{x}_s) + \sum_{s,k} \alpha_s^*\alpha_k^*(\mathbf{x}_s \cdot \mathbf{x}_k) \leq R^{*2} \quad (14)$$

where s and k are indices of the support vectors in the set S.

The primary SVDD method can be extended by replacing the inner product $(\mathbf{x}_i \cdot \mathbf{x}_j)$ by a Gaussian kernel function $K_G(\mathbf{x}_i, \mathbf{x}_j) = \exp(-\|\mathbf{x}_i - \mathbf{x}_j\|^2/\sigma^2)$ [22]. Substituting the Gaussian kernel function into (13) leads to the Lagrangian

$$\hat{L} = 1 - \sum_i \alpha_i^2 - \sum_{i\neq j} \alpha_i\alpha_j K_G(\mathbf{x}_i, \mathbf{x}_j). \quad (15)$$

Maximizing the Lagrangian $\hat{L}$ gives the set S that contains support vectors $\mathbf{x}_s$ with the corresponding $\alpha_s^* \neq 0$. The center of the support vectors is then given by

$$\mathbf{a}^* = \sum_s \alpha_s^* \mathbf{x}_s \text{ where } \mathbf{x}_s \in S. \quad (16)$$

The radius R^* is computed by choosing one of the support vectors $\mathbf{x}_t \in S$

$$R^{*2} = 1 - 2\sum_s \alpha_s^* K_G(\mathbf{x}_s, \mathbf{x}_t) + \sum_{s,k} \alpha_s^*\alpha_k^* K_G(\mathbf{x}_s, \mathbf{x}_k) \quad (17)$$

where $\mathbf{x}_s, \mathbf{x}_k \in S$. Furthermore, a test point $\mathbf{z}$ is considered inside the boundary when the following inequality is satisfied:

$$K_G(\mathbf{z},\mathbf{z}) - 2\sum_s \alpha_s^* K_G(\mathbf{z}, \mathbf{x}_s) + \sum_{s,k} \alpha_s^*\alpha_k^* K_G(\mathbf{x}_s, \mathbf{x}_k) \leq R^{*2} \quad (18)$$

where $\mathbf{x}_s, \mathbf{x}_k \in S$.

The number of support vectors can be adjusted by two parameters: the weight C in (7) and the width σ in the Gaussian kernel K_G. Parameter C is not critical in practice [22], hence we will determine σ. To see the effect of σ on the selection of the support vectors, let us consider a very small σ. In this case

$$K_G(\mathbf{x}_i, \mathbf{x}_j) = \exp\left(\frac{-(\mathbf{x}_i - \mathbf{x}_j)^2}{\sigma^2}\right) \simeq 0$$

when $i \neq j$. Equation (15) becomes $\hat{L} = 1 - \sum_i \alpha_i^2$, which is maximized when all $\alpha_i^* = (1/N)$. In this situation, all the data points in the cluster become support vectors, and no compression is achieved. For a very large σ, $K_G(\mathbf{x}_i, \mathbf{x}_j) \simeq 1$, then (15) becomes $\hat{L} = 1 - \sum_i \alpha_i^2 - \sum_{i\neq j} \alpha_i\alpha_j$, which is maximized by letting only one $\alpha_i^* = 1$ for any i and all the other α_j where $j \neq i$ to be zero. Hence, only one data point will be selected to represent the entire cluster.

REFERENCES

[1] N. E. Leonard, D. A. Paley, R. E. Davis, D. M. Fratantoni, F. Lekien, and F. Zhang, "Coordinated control of an underwater glider fleet in an adaptive ocean sampling field experiment in Monterey bay," *J. Field Robot.*, vol. 27, no. 6, pp. 718–740, 2010.

[2] N. E. Leonard, D. A. Paley, F. Lekien, R. Sepulchre, D. M. Fratantoni, and R. E. Davis, "Collective motion, sensor networks, and ocean sampling," *Proc. IEEE*, vol. 95, no. 1, pp. 48–74, Jan. 2007.

[3] B. Garau, A. Alvarez, and G. Oliver, "Path planning of autonomous underwater vehicles in current fields with complex spatial variability: An A* approach," in *Proc. IEEE Int. Conf. Robot. Autom.*, 2005, pp. 194–198.

[4] A. Alvarez, A. Caiti, and R. Onken, "Evolutionary path planning for autonomous underwater vehicles in a variable ocean," *IEEE J. Ocean. Eng.*, vol. 29, no. 2, pp. 418–429, Apr. 2004.

[5] T. Lolla, M. Ueckermann, K. Yigit, P. Haley, Jr., and P. F. Lermusiaux, "Path planning in time dependent flow fields using level set methods," in *Proc. IEEE Int. Conf. Robot. Autom.*, 2012, pp. 166–173.

[6] C. Petres, Y. Pailhas, P. Patron, Y. Petillot, J. Evans, and D. Lane, "Path planning for autonomous underwater vehicles," *IEEE Trans. Robot.*, vol. 23, no. 2, pp. 331–341, Apr. 2007.

[7] S. L. X. Francis, S. G. Anavatti, and M. Garratt, "Real time cooperative path planning for multi-autonomous vehicles," in *Proc. Int. Conf. Adv. Comput., Commun. Informat.*, Aug. 2013, pp. 1053–1057.

[8] M. Shanmugavel, A. Tsourdos, B. White, and R. Zbikowski, "Co-operative path planning of multiple UAVs using Dubins paths with clothoid arcs," *Control Eng. Pract.*, vol. 18, no. 9, pp. 1084–1092, 2010.

[9] D. Stilwell, B. Bishop, and C. Sylvester, "Redundant manipulator techniques for partially decentralized path planning and control of a platoon of autonomous vehicles," *IEEE Trans. Syst., Man, Cybern. B, Cybern.*, vol. 35, no. 4, pp. 842–848, Aug. 2005.

[10] N. Baccour *et al.*, "Radio link quality estimation in wireless sensor networks: A survey," *ACM Trans. Sensor Netw.*, vol. 8, no. 4, 2012, Art. no. 34.
[11] M. Stojanovic, "Optimization of a data link protocol for an underwater acoustic channel," in *Proc. IEEE Oceans*, 2005, vol. 1, pp. 68–73.
[12] R. Hoffman and E. Krotkov, "Terrain roughness measurement from elevation maps," in *Proc. Adv. Intell. Robot. Syst. Conf.*, 1989, pp. 104–114.
[13] D. B. Gennery, "Traversability analysis and path planning for a planetary rover," *Auton. Robots*, vol. 6, no. 2, pp. 131–146, 1999.
[14] S. Singh *et al.*, "Recent progress in local and global traversability for planetary rovers," in *Proc. IEEE Int. Conf. Robot. Autom.*, 2000, vol. 2, pp. 1194–1200.
[15] A. Howard and H. Seraji, "Vision-based terrain characterization and traversability assessment," *J. Robot. Syst.*, vol. 18, no. 10, pp. 577–587, 2001.
[16] C. Ye, "Navigating a mobile robot by a traversability field histogram," *IEEE Trans. Syst., Man, Cybern. B, Cybern.*, vol. 37, no. 2, pp. 361–372, Apr. 2007.
[17] J. Larson, M. Trivedi, and M. Bruch, "Off-road terrain traversability analysis and hazard avoidance for UGVs," Dept. Electr. Eng., Univ. California, San Diego, CA, USA, pp. 1–7, 2011.
[18] P. Papadakis, "Terrain traversability analysis methods for unmanned ground vehicles: A survey," *Eng. Appl. Artif. Intell.*, vol. 26, no. 4, pp. 1373–1385, 2013.
[19] D. Joho, C. Stachniss, P. Pfaff, and W. Burgard, "Autonomous exploration for 3D map learning," in *Autonome Mobile Systeme 2007*. New York, NY, USA: Springer-Verlag, 2007, pp. 22–28.
[20] S. Choi, E. Kim, and S. Oh, "Real-time navigation in crowded dynamic environments using Gaussian process motion control," in *Proc. IEEE Int. Conf. Robot. Autom.*, May 2014, pp. 3221–3226.
[21] Y. Tanaka, Y. Ji, A. Yamashita, and H. Asama, "Fuzzy based traversability analysis for a mobile robot on rough terrain," in *Proc. IEEE Int. Conf. Robot. Autom.,* 2015, pp. 3965–3970.
[22] D. M. Tax and R. P. Duin, "Support vector data description," *Mach. Learn.*, vol. 54, no. 1, pp. 45–66, 2004.
[23] S. Liu, J. Yu, A. Zhang, and F. Zhang, "Cooperative path planning for networked gliders under weak communication," in *Proc. Int. Conf. Underwater Netw. Syst.*, 2014, Paper 5.
[24] S. Liu, J. Yu, A. Zhang, and F. Zhang, "An adaptive scheme of sharing compressed flow information among networked underwater gliders," in *Proc. IEEE Int. Conf. Cyber Technol. Autom., Control, Intell. Syst.*, Jun. 2015, pp. 1115–1120.
[25] F. Zhang, D. M. Fratantoni, D. A. Paley, J. M. Lund, and N. E. Leonard, "Control of coordinated patterns for ocean sampling," *Int. J. Control*, vol. 80, no. 7, pp. 1186–1199, 2007.
[26] L. M. Merckelbach, R. D. Briggs, D. A. Smeed, and G. Griffiths, "Current measurements from autonomous underwater gliders," in *Proc. IEEE Work. Conf. Current Meas. Technol.*, 2008, pp. 61–67.
[27] "Date source form hycom," 2017. [Online]. Available: http://tds.hycom.org/thredds/GLBv0.08/expt_92.8.html
[28] D. Chang, X. Liang, W. Wu, C. R. Edwards, and F. Zhang, "Real-time modeling of ocean currents for navigating underwater glider sensing networks," in *Cooperative Robots and Sensor Networks*. Berlin, Germany: Springer-Verlag, 2014, pp. 61–75.
[29] P. Qarabaqi and M. Stojanovic, "Statistical characterization and computationally efficient modeling of a class of underwater acoustic communication channels," *IEEE J. Ocean. Eng.*, vol. 38, no. 4, pp. 701–717, Oct. 2013.
[30] K. Cho and D. Yoon, "On the general Ber expression of one-and two-dimensional amplitude modulations," *IEEE Trans. Commun.*, vol. 50, no. 7, pp. 1074–1080, Jul. 2002.
[31] F. Bretherton, R. Davis, and C. Fandry, "A technique for objective analysis and design of oceanographic experiments applied to MODE-73," *Deep Sea Res. Oceanogr. Abstr.*, vol. 23, no. 7, pp 559–582, Jul. 1976.

Shijie Liu (S'18) received the B.S. degree in electrical and information engineering from Anhui Normal University, Wuhu, China, in 2012. He is currently working toward the Ph.D. degree in mechatronic engineering at the Shenyang Institute of Automation, Chinese Academy of Sciences, Shenyang, China.

His research interests include mobile sensing for ocean observation and marine autonomy.

Jie Sun received the B.S. degree in marine technology and the M.S. degree in acoustics from the Ocean University of China, Qingdao, China, in 2011 and 2014, respectively. She is currently working toward the Ph.D. degree in mechatronic engineering at the Shenyang Institute of Automation, Chinese Academy of Sciences, Shenyang, China.

Her research interests include acoustic theory and technology for marine robots and mobile sensor networks.

Jiancheng Yu received the B.S. degree in mechanical engineering and the M.S. degree in mechanical design and theory from Northeastern University, Shenyang, China, in 2000 and 2003, respectively, and the Ph.D. degree in mechatronic engineering from the Shenyang Institute of Automation, Chinese Academy of Sciences, Shenyang, China, in 2006.

He is a Professor at the Shenyang Institute of Automation. His research interests include control theory and methods research for underwater vehicles and new concept underwater vehicles design.

Aiqun Zhang received the B.S. degree in mechanical engineering from Northeastern University, Shenyang, China, in 1982.

He spent more than 30 years developing underwater vehicles, first as the Director of the Marine Robotics Department, Shenyang Institute of Automation, Chinese Academy of Sciences, Shenyang, China, and, more recently, as the Engineer-in-Chief at the Institute of Deep-Sea Science and Engineering, Chinese Academy of Sciences, Sanya, China. His research interests include overall design for underwater vehicles and technologies for extremely deep sea exploration.

Fumin Zhang (S'01–M'04–SM'13) received the B.S. and M.S. degrees from Tsinghua University, Beijing, China, in 1995 and 1998, respectively, and the Ph.D. degree in electrical and computer engineering from the University of Maryland, College Park, MD, USA, in 2004.

In 2007, he joined the School of Electrical and Computer Engineering, Georgia Institute of Technology, Atlanta, GA, USA, where he is currently a Professor. From 2004 to 2007, he was a Lecturer and a Postdoctoral Research Associate at the Mechanical and Aerospace Engineering Department, Princeton University, Princeton, NJ, USA. His research interests include marine autonomy, mobile sensor networks, and theoretical foundations for battery supported cyber-physical systems.

Dr. Zhang received the National Science Foundation (NSF) CAREER Award in 2009 and the Office of Naval Research (ONR) Young Investigator Program (YIP) Award in 2010.